THEORETICAL VS. ACTUAL MUD MOTOR PERFORMANCE IN UNCONVENTIONAL FORMATIONS AND STRATEGIES TO EXTEND MOTOR LIFE

A Thesis

by

IBRAHIM SAMI EL-SAYED

Submitted to the Office of Graduate and Professional Studies of
Texas A&M University
in partial fulfillment of the requirements for the degree of

MASTER OF SCIENCE

Chair of Committee,	Sam Noynaert
Committee Members,	Eduardo Gildin
	Mathew Kuttolamadom
Head of Department,	Jeff Spath

August 2018

Major Subject: Petroleum Engineering

ABSTRACT

The continued growth in unconventional drilling has pushed motors to drill more complex geometries, drill faster, and drill at higher well temperatures. The most common method to postpone motor failure has been to select a larger motor. This option ignores the root causes of motor failure and would leave performance on the table. Impetus for this work centered around an operator in the Eagleford who was experiencing high rates of motor failure. In the process of investigating the failures, important findings were made that apply to any BHA with a motor.

Motor properties are used to convert the traditional surface MSE measurement into a more representative bit MSE. Bit MSE is calculated using, a simple factor and a more exact but complicated multi-dimensional correlation. Drilling data is used to show that the simplicity of the simple factor more than offsets minor loses in MSE accuracy. The realtime RPM factors are also computed using downhole data showing the stark differences between the actual factors and the originally reported factors. The difference is used to determine the degree of motor damage while drilling.

A suite of downhole sensors are placed above and below the motor to monitor the rate of motor damage. Differential pressure is also analyzed in the frequency domain spectrum to demonstrate the damaging effect of bottomhole assembly (BHA) whirl during rotating. However, bit MSE does not provide an accurate indication of the degree of whirl occurring in the motor. Rather, a BHA must be engineered to minimize motor vibrations and damage. Correspondingly, an empirical equation is derived to predict the fundamental differential pressure frequency of a motor.

The use of depth of cut control (DOCC) is analyzed as a method to improve motor efficiency and decrease damage. Two identical wells and BHA's are compared, one with and one without DOCC. The uses of the first derivative of differential pressure is suggested as a method to better quantify and visualize the effects of DOCC. Ultimately, the research presented provides quantitative insights into the operation of a motor, and changes are proposed to improve motor life based on the observed data.

CONTRIBUTORS AND FUNDING SOURCES

This work was supported by a dissertation committee consisting of Professor Sam Noynaert [advisor] and Fred Dupriest of the Department of Petroleum Engineering and Professor Mathew Kuttolamadom of the Department of Engineering Technology & Industrial Distribution

All work conducted for the dissertation was completed by the student independently.

Graduate study was supported by a Graduate Assistant Research position funded by Marathon Oil.

NOMENCLATURE

Dia	bit diameter (in)
GPM	mud flow rate (gal/min)
MSE	mechanical specific energy (kpsi)
PDiff	differential pressure (psi)
RF	RPM factor (rev/gal)
RPM	revolutions per minute (rpm)
ROP	rate of penetration (ft/hr)
TF	torque factor (ft-lbs/psi)
Tor	Top Drive torque (ft-lbs)
WOB	weight on bit (klbf)
π	pi

TABLE OF CONTENTS

Page

LIST OF FIGURES

Page

1. INTRODUCTION

Drilling in the Eagleford, Marathon has experienced a large number of mud motor failures. This is in part due to the bottomhole temperatures, ranging from 280°F to 320°F, which weakens the rubber (Beeh et al. 2018). Typical lateral motor and drilling conditions can be seen in **Table 1**. The simplest approach to power section related failures has been to select a larger motor. A power section that is larger in diameter or features more stages will fatigue at relatively slower rate and tend to have a successful run (Guidroz et al. 2011). However, this solution is limited for four key reasons. First, it takes time to design and engineer new power sections. Second, this solution only delays the onset of problems. As operators drill longer, deeper, hotter wells, the failures will reemerge. Third, when provided with a more powerful motor, operators will run the motor at the high specifications leading to damage just as quickly. This effect is illustrated in **Fig. 1** with the recent introduction of larger 11.2 stage motors over the past year. Despite the use of a larger motor, failure rates remain relatively constant.

Lateral Length	3,000ft - 8,000ft
Bottom Hole Temperature	280°F - 320°F
Motor Lobe Configuration	5/6 or 7/8
Motor Bend Angle	2.12°
Motor Number of Stages	6.8, 9.4, 10.8, 11.2
Motor Diameter	7"
Motor Bit to Bend	4.5 ft - 5.5 ft
Motor Stabilization	None
Desired Build Rate	10°/100ft - 14°/100ft

Table 1: Typical range of parameters and conditions for the motors run by Marathon.

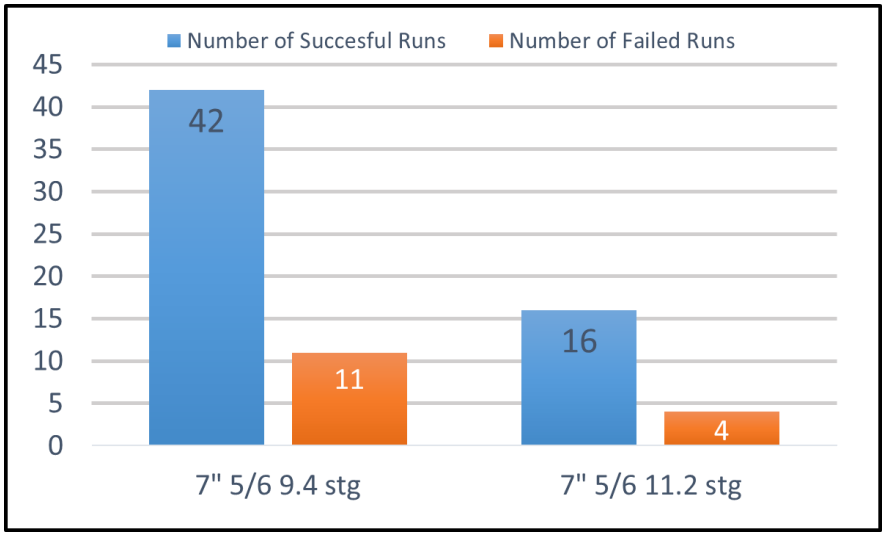

Fig. 1: Despite the recent introduction of a larger motor, failure rates still remain at around 20%. Data based on motors over a one-year period from May 2017 to June 2018.

In addition, even the motors that do not fail are severely damaged due to rubber chunking. This can be seen in **Fig. 2,** where the chunking is much more severe at the bottom of the motor. With this degree of damage, it begs the question, how much can performance be improved if this damage was mitigated? Therefore, the purpose of the current work is to analyze motor performance during operation by using high frequency downhole data and mechanical specific energy (MSE) monitoring so as to extend the operating window of any motor.

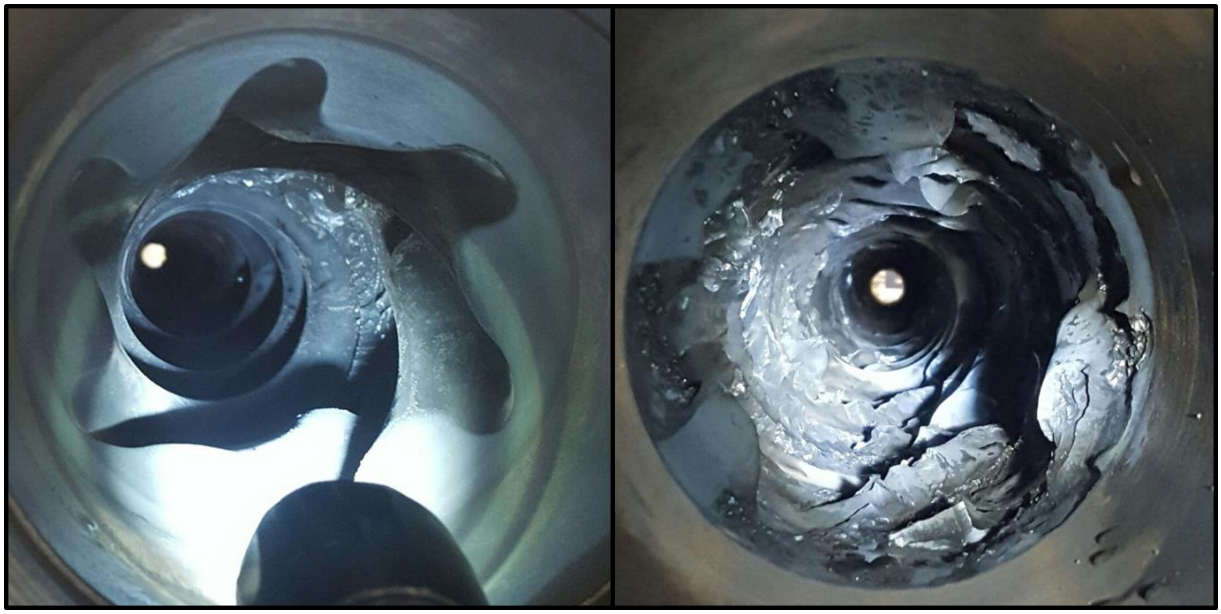

Fig. 2: Damage is much more severe on the bottom of the motor (right) as compared to the top of the motor (left).

2. LITERATURE REVIEW

Mud motors are the tool of choice for U.S. unconventional drilling (Ba et al. 2016). They provide a cheap and reliable method to build high angle wells quickly. Mud motors' components can be divided into two sections, the power section and the bent housing/ transmission. Whereas the bent housing allows for the mud motor to provide directional work, the power section—a positive displacement motor (PDM)—provides the increased drilling power (Hendrik 1997). The PDM mechanism has been long established and is fundamentally the inverse of a progressive cavity pump (Moineau, 1939). However, even though the basic mechanism is well understood, it remains the focus of much technological improvement and in-depth analysis to further model downhole operations.

A PDM is composed of a rotor within a stator. The stator's inner surface is lined with rubber and is contoured into several lobes that helix down the length of the stator. In contrast, the stator is typically hard faced to reduce wear. In order to allow fluid flow through the motor, the stator features one less lobe that helixes at the same pitch as the rotor (Hohl et al. 2017). The power section is often categorized by factors such as its diameter, number of stages, number of lobes, and the interference fit between the stator and rotor (Beeh et al. 2018). A cross section of a power section can be seen in **Fig. 3**.

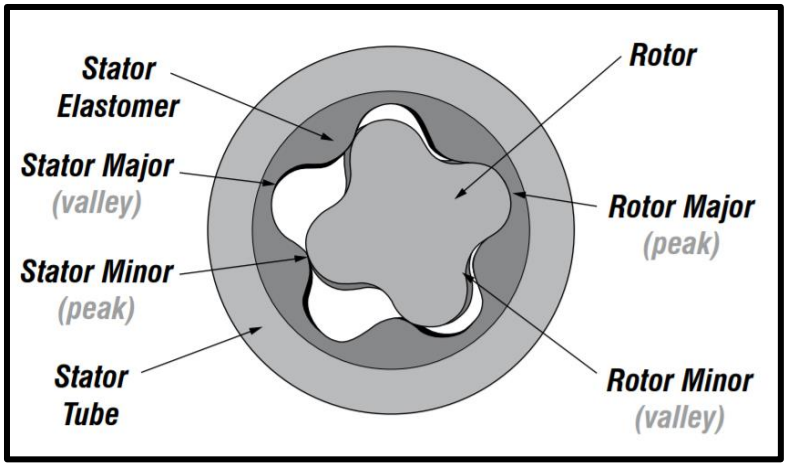

Fig. 3: Illustration of stator and rotor configuration (Dyck 2011).

As the fluid flows through the motor the difference in lobe numbers between the rotor and the stator causes discrete cavities to form. The pressure differences within each discrete fluid cavity cause the rotor to spin in an erratic pattern that is transferred into smooth rotation by the transmission section (Jaeger and Herlitzius, 2016). For 100% efficiency the cavities should remain hydraulically sealed; however, slippage can occur due to high differential pressure, improper rotor-stator fit and wear toward the end of a motor's run. Minor leakage can be advantageous and is designed into some motors as it can lubricate the power section, reduce overall friction, and cool the stator. Major leakage will reduce the efficiency of the motor and could potentially accelerate motor erosion (Ba et al. 2016).

Motor failure while drilling can occur in the power section or in the bearing/transmission assembly. Of these, power section failures are more complex and less likely to be clearly understood. Failures in the bearing/transmission assembly are typically caused by excessive stickslip. The speed oscillations cause the metal components to smash together violently until failure. However, with proper system design and operational practices, stickslip can be mitigated

and this damage alleviated. Unsurprisingly, failures are more common in the power section due to the presence of rubber in the stator. While the failure methods for the rubber vary, they fundamentally involve rubber fatiguing. Fatigue is brought on due to a combination of cyclical loading and temperature weakening (Ba et al. 2016). Delpassand (1999), Gamboa et al. (2003), Hohl et al. (2015), and Ba et al. (2016) are examples of works quantifying motor failures through numerical models. Of these, Ba et al. is the most recent and relevant to our work. His work modeled motor power section fatigue as a function of several parameters such as differential pressure, flow rate, interference fit, downhole temperature, and elastomer type. The models did not take into account potential inefficiencies in the drilling system due to these changes. For example, for the motor modeled, a 20% decrease in differential pressure would increase motor life by 250%. A decrease in differential pressure would also indicate a decrease in WOB and bit engagement. Therefore, whirl could become less suppressed which could induce damaging vibrations in the bit and motor (Dupriest and Koederitz 2002).

Mechanical Specific Energy (MSE) for drilling was first defined by Teale as the energy needed to remove a unit volume of rock (1965). It is derived by Teale in **Eq. 1** and **Eq. 2** below.

$$MSE_{Surface} = \frac{Input\ Energy}{Output\ Rock\ Volume\ Removed} \quad \text{..... (1)}$$

$$MSE_{suface} = \frac{480 * Tor * total\ RPM}{Dia^2 * ROP} + \frac{4 * WOB}{Dia^2 * \pi} \quad \text{..... (2)}$$

At 100% efficiency, such as that found in lab-scale drilling, it was found that the MSE would equal the rock compressive strength (Teale 1965). In the special case of ductile rather than brittle material failure, MSE will be roughly three times rock strength (Rafatian et al. 2009). However,

the absolute value of MSE is very much secondary to its relative value. This is because in an actual drilling system, numerous inefficiencies will exist. Thus, MSE is utilized in real time drilling analysis to provide a strong indicator of when the bit is drilling efficiently and most importantly, what changes to drilling parameters either improve or hurt said efficiency. Most cutting inefficiency can be traced to vibrations. This is proven through several studies that show that MSE is an excellent indicator of downhole vibrations including induced dysfunctions such as whirl and stickslip (Dupriest and Koederitz 2002; Pessier and Fear 1992; Fei et al. 2017). However, a limitation of $MSE_{Surface}$ is that the industry currently uses surface data as an input. In high angle or horizontal wells, the surface torque is a combination of the torque used to drill and the torque caused by friction between the borehole and drill pipe. There is no clear way to differentiate the bit torque component from the friction loss torque component. While this can be performed using downhole sensors, unconventional oil and gas drilling operations typically utilize telemetry systems that cannot communicate at a high enough data rate to calculate real time MSE at an acceptable frequency (1 hz or faster). Thus, MSE from downhole sensors can be found post-run rather than in real time. If drilling with a mud motor, another limitation of $MSE_{Surface}$ is that it provides no information while sliding because the top drive is not providing surface RPM and torque. However, the presence of a mud motor in the bottom hole assembly (BHA) does provide the unique opportunity to acquire an accurate downhole MSE value without the use of sensors. By using surface pressure data, as shown in Eqn. 2, along with key properties of the motor, a relatively accurate MSE_{Bit} can be calculated that gives a much clearer picture of drilling efficiency, even when drilling long laterals or at high angles.

Every power section is rated under surface conditions regarding the output rpm and output torque as functions of the flow rate and differential pressure. A typical example of this can be seen in

Fig. 4. Output motor torque is theoretically linear with the differential pressure across the motor. The slope of this line is the torque factor and can be used to convert differential pressure to motor torque. However, models have shown that the linearity diminishes at higher differential pressures The range of the linear region is dependent on the elastomer used (Ba et al. 2016). In contrast, the output rpm is more dynamic is it depends on the flow rate and the load conditions as indicated by differential pressure. As differential pressure increases, the load increases on the motor and results in a decrease in output rpm. The rate of drop-off depends on the elastomer type and lobe configuration. However, most motor data sheets assume this drop off to be negligible and report a revolution per minute (rpm) factor based on no load conditions (Macpherson and Jogi 2001). Additionally, both factors can be impacted due to motor operation. Operational fatigue, rubber damage, and fluid slippage can alter the linear torque and RPM factors, especially as the components wear and tolerances get larger over the length of a particular BHA (Gamboa, 2003). These effects are common knowledge but specific guidance on how to quantify them or models showing such effects are limited and were found to not have an application for this study (Samuel and Miska 1997).

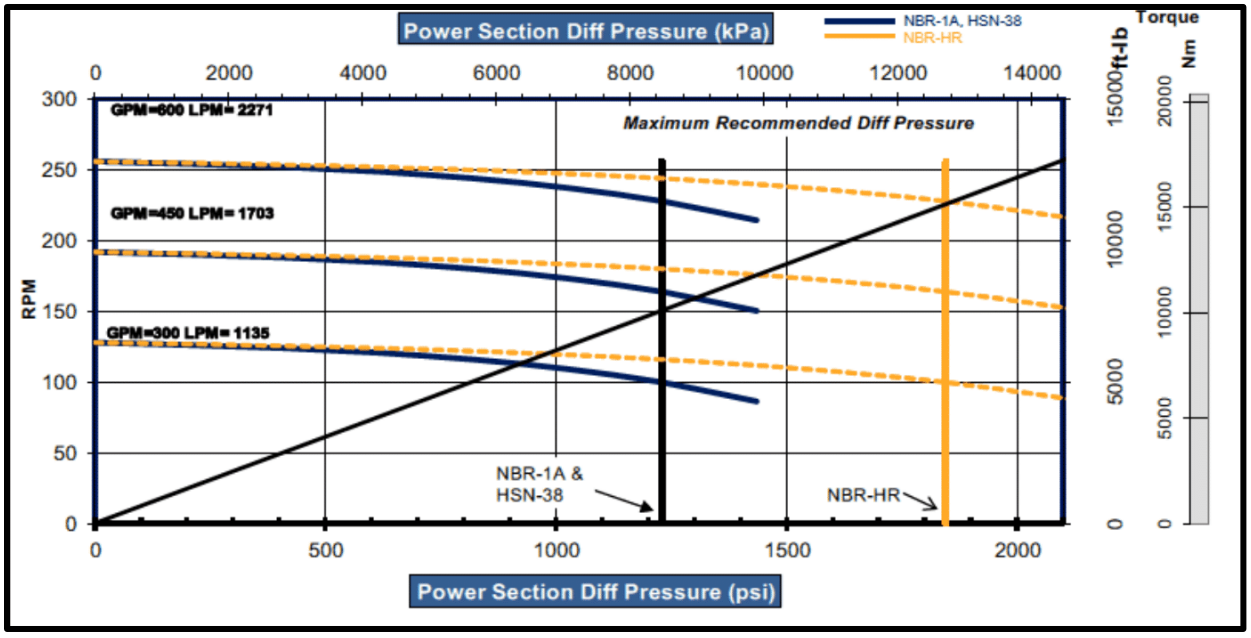

Fig. 4: Standard mud motor power curve illustrating the relationship between input differential pressure and output torque and rpm.

Using these factors, the $MSE_{Surface}$ equation using surface data form Eqn. 2 is manipulated into an MSE_{Bit} equation that utilizes motor torque and motor rpm. Because the motor is relatively close to the bit as compared to the surface, it is safe to assume that this torque and rpm are nearly identical to the bit torque and bit RPM. This new MSE equation will be denoted as the MSE_{Bit} and can be seen in Eqn. 3.

$$MSE_{Bit} = \frac{480*(TF*P_{Diff})*((RF*GPM)+RPM)}{Dia^2*ROP} + \frac{4*WOB}{Dia^2*\pi} \quad \text{.....(3)}$$

MSE_{Bit} can now be used to perform the same functions and insights as $MSE_{Surface}$ for vertical or deviated hole in identifying drilling efficiency and dysfunction. However, the use of MSE_{Bit} in real time or post run analysis provides two new benefits.

First, MSE_{Bit} allows for MSE monitoring during sliding. It is normal to observe that MSE_{Bit} will decrease when sliding as compared to when rotating. This is caused by the bent nature of a mud motor. When rotating the motor will cause the bit to spin off center and will drill an over-gauge hole (Hohl et al. 2017). Because of this mass imbalance, whirl is inevitable while rotating and an increase in MSE_{Bit} is consistently observed. When sliding, all rotation occurs below the bent housing and the mass imbalance is eliminated. This is illustrated in **Fig. 5**. Remmert et al. (2007) and Bybee (2010) have demonstrated that there can be significant gains in ROP by reducing and eliminating bend angles. This improvement in ROP comes as a direct result of reducing bit whirl.

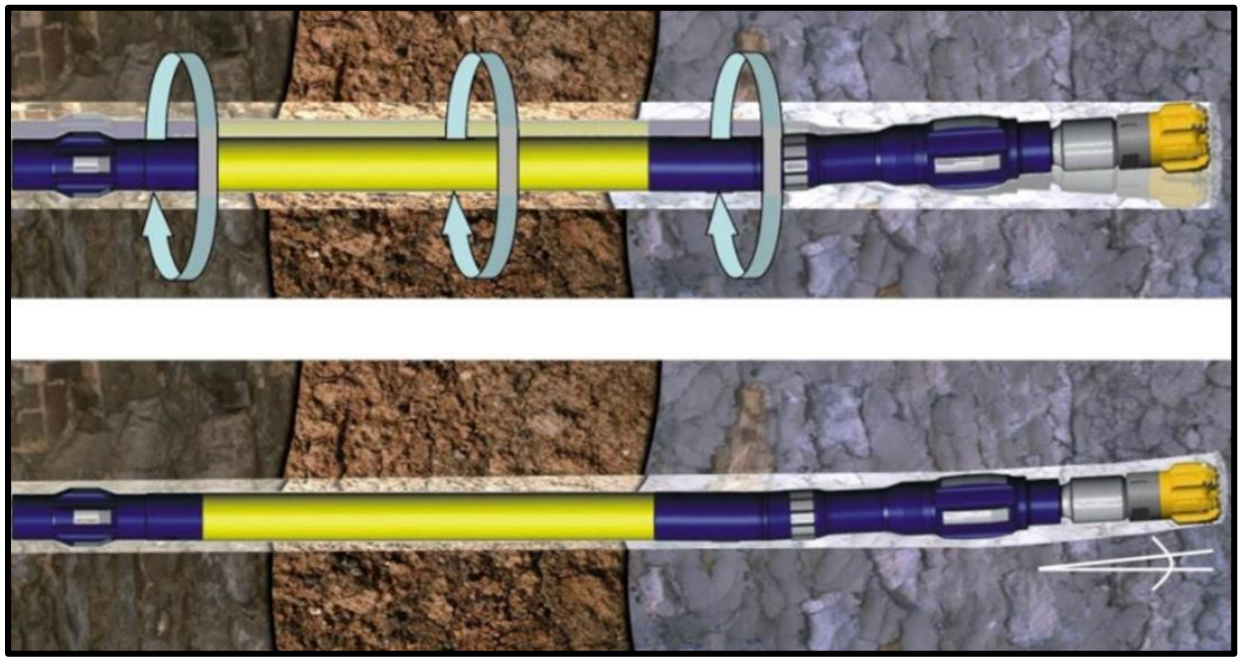

Fig. 5: While rotating the motor bend angle creates a mass imbalance that results in greater downhole whirl and an over gauge hole. While sliding this is eliminated (Jaeger and Herlitzius 2017).

Second, MSE_{Bit} can be used in conjunction with $MSE_{Surface}$ to identify weight transfer issues. The surface torque is the summation of the drilling torque and torque due to friction between the pipe and borehole. In a perfectly efficient system, an increase in drilling should manifest itself in

both $MSE_{Surface}$ MSE_{Bit}. However, no wells, particularly horizontal wells, are efficient in transmitting energy to the bit. Thus if MSE_{Bit} remains constant and an increase in $MSE_{Surface}$ is observed, this is likely caused by inefficient weight transfer to the bit. An example of this can be seen in **Fig. 6** where a pair of short slides created ledges during the slide to rotate transition that caused the BHA to hang up and reduced weight transfer.

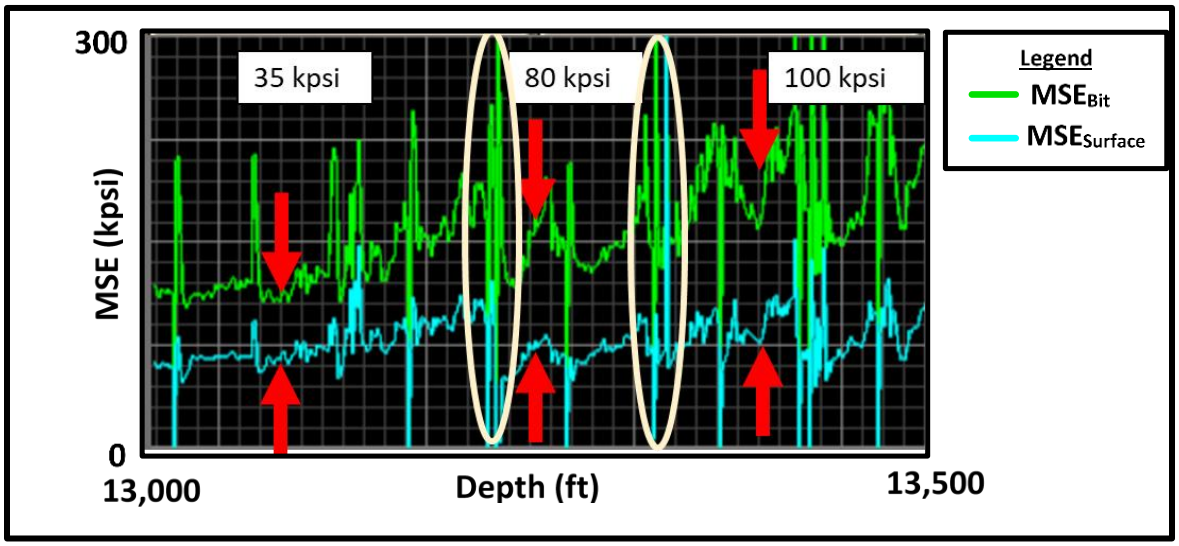

Fig. 6: Weight transfer issues can be identified by comparing the change in the gap between MSE_{Bit} and $MSE_{Surface}$. Weight transfer problems where made worse by two short slides (circled).

3. BIT MSE RELIABILITY

MSE_{Bit} is calculated using simple motor factors for rpm and torque. The simplicity allows for quick MSE_{Bit} analysis and for real time plotting on the rig's Electronic Drilling Recorder (EDR) display. However, as previously discussed, the power section's rotor stator interaction is much more complicated than to be described by a pair of linear factors. Does the tradeoff in accuracy for simplicity reduce the integrity of MSE_{Bit}?

To analyze this, a motor power curve, shown in Fig. 4, was used to generate a multi-dimensional correlation that more precisely modeled the motor output rpm using flow rate and differential pressure as inputs. Motor speed was calculated using the RPM factor times the flow rate as shown in. Eq. 4. The data sheet for this specific motor listed a RPM factor of .426 rev/gal and the multi-dimensional accurate RPM factor correlation, is shown in Eq. 5 and **Fig. 7** where RF refers to the RPM factor and GPM refers to the mud flow rate in gallons per minute or gal/min. Just as how different motors have different RPM factors, this correlation was constructed for a specific motor.

$$Motor\ Speed = RF * GPM \quad \text{.....(4)}$$

$$RF_{accurate} = \left(-1.398e-11 * {P_{Diff}}^3\right) + \left(8.928-11 * {P_{Diff}}^2 * GPM\right) + \left(-2.411e-10 * P_{Diff} * GPM^2\right) + \left(-5.283e-8 * {P_{Diff}}^2\right) + \left(2.436e-7 * P_{Diff} * GPM\right) + (1.682e-8 * GPM^2) + \left(-7.664-5 * P_{Diff}\right) + (-2.278e-5 * GPM) + .4349 \quad \text{.....(5)}$$

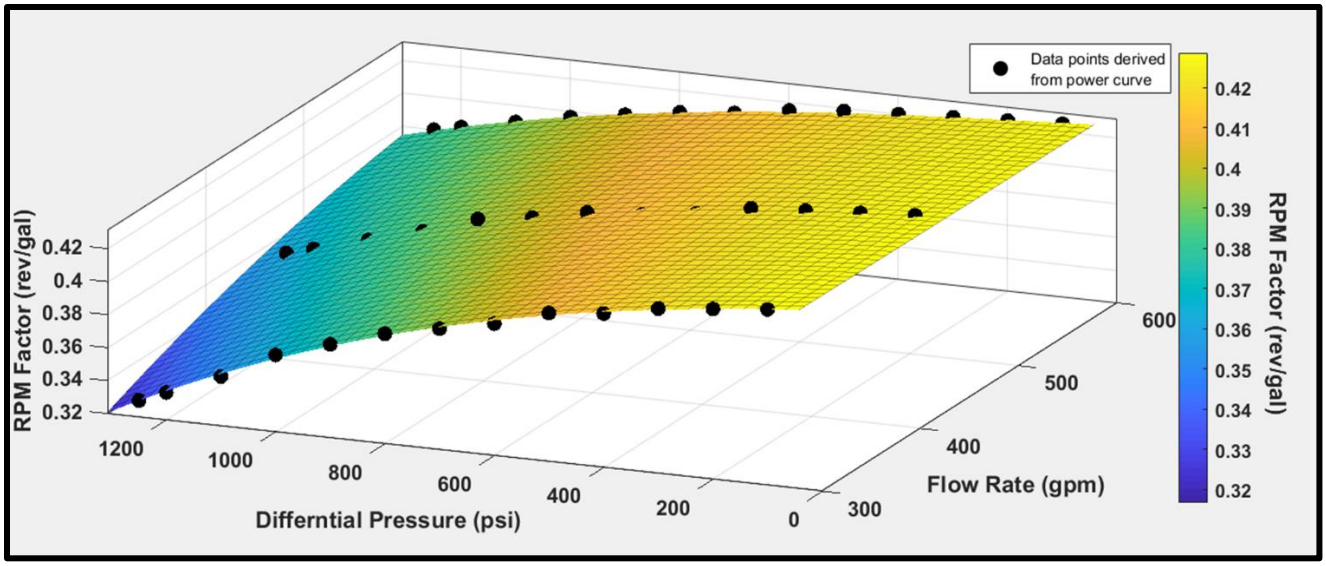

Fig. 7: Eqn. 5 presented in graphical format. APM Factors are lowest at high differential pressures and low flow rates.

Drilling data was then analyzed post run and MSE_{Bit} calculated using both the basic factor and the accurate correlation. The percent error between the two measurements is shown in **Fig. 8**. Overall the change in MSE_{Bit} averaged less than 3%. In addition, the spread of the error is minimal such that the error never exceeded 8%. Hence, using a simple factor provides an accurate representation of MSE_{Bit} across all drilling. Given the standard sensors and data acquisition rates on typical land rigs, one can assume other sources of error overshadow the effect of using more accurate MSE_{Bit} calculation . The largest relative errors were observed at low flow rates and high differential pressures. The former is typically avoided as operators opt to maximize flow rate to improve hole cleaning. Additionally, because the reported RPM factor was based off of the no load condition, the correlation-based RPM factor was consistently lower resulting in reduced bit speed and reduced calculated bit MSE_{Bit}. Thus, the uncorrected MSE_{Bit} will always show the driller the higher, worse-case value.

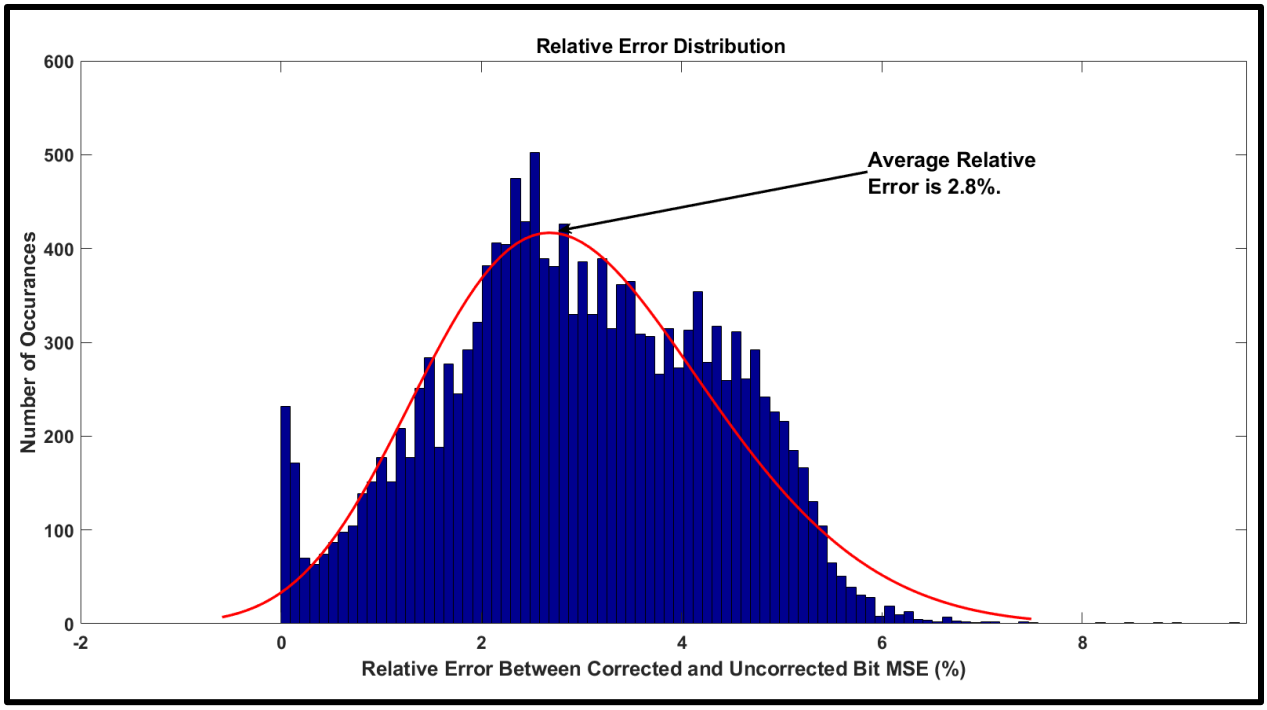

Fig. 8: Data from an entire run is compared using the corrected and uncorrected MSE_{Bit}. The overall calculated error is minimal

Therefore, if a motor power curve is accurate, using a single RPM factor simplifies the MSE_{Bit} equation while maintaining the data integrity and does so with an equation that is easy to program into real time drilling data monitoring systems.

The prior discussion predisposes that the motor curves provided are accurate which the authors found is not always the case. Beeh et al. (2018) also noted the potential inaccuracies in power curves using modeling rather than a data driven approach **Fig. 9** depicts a motor that featured a gyro sensor in the bit box measuring rpm. The actual, measured rpm was far below the expected rpm that one would find using the no load reported RPM factor of 0.4 revolutions per gallon or rev/gal. The measured RPM correlated to an RPM factor of ~0.28 rev/gal: 30% less than the reported RPM factor. Moreover, by analyzing the motor power curve, a precise theoretical RPM factor for the operating conditions of 750 gpm and 800 psi was calculated to be 0.39 rev/gal, an

insignificant change. Even a worst-case scenario from the motor specification sheet—low flow rate with high differential pressure—only yielded an RPM factor of .31 based on the reported power curves.

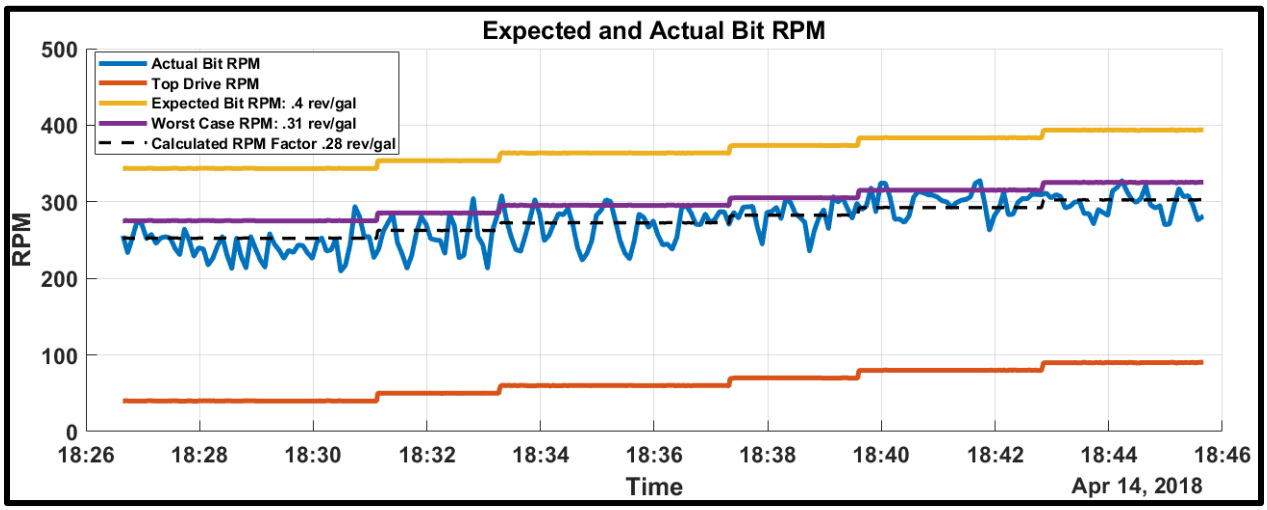

Fig. 9: Downhole RPM is significantly less than what is expected using the reported RPM factors and any other RPM factors derived from the motor power curve.

However, the decreased apparent RPM factor is not an isolated problem. **Fig. 10** shows that the calculated RPM factor for the motor was constantly decreasing throughout the entire run. This can be understood as increased damage in the power section resulting in reduced performance. Initially, the RPM factor was near the reported values as per the power curves. Shortly after completing the curve portion of the well, the rate of deterioration in the RPM factor increased significantly. As the motor enters the lateral portion of the well, it is primarily operated in the rotating drilling mode as opposed to the sliding drilling mode. As previously discussed, drilling with a motor while rotating results in higher vibrations, shown in Fig. 5, due to the inherent mass imbalance (Hohl et al. 2017). Therefore, it reasons that the presence of increased whirl while rotating accelerates the rate of rubber damage in the power section and decreases the

performance of the motor. This would explain the decreased performance as the motor entered the lateral portion of the well.

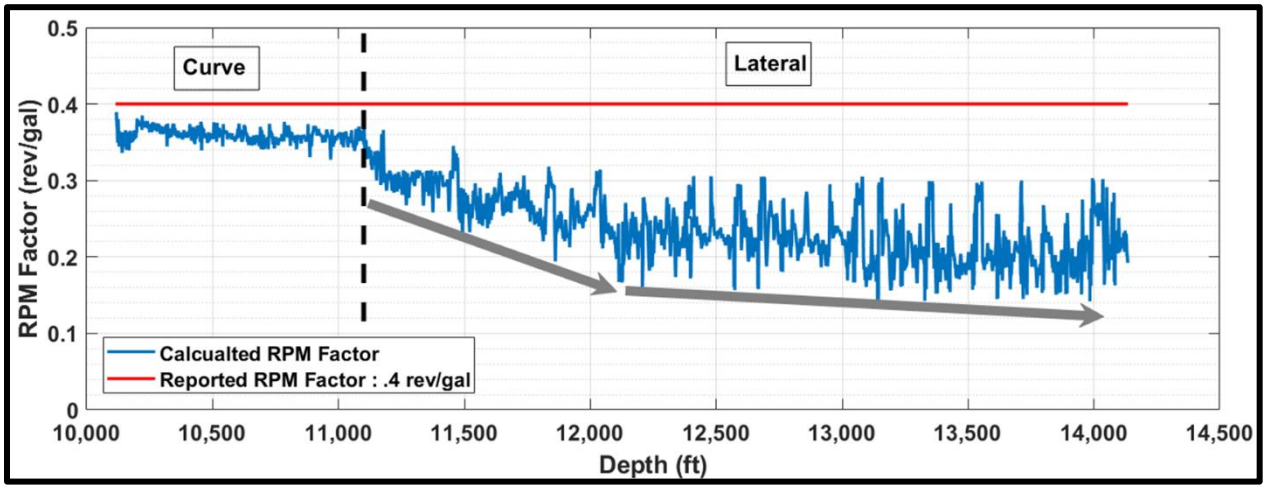

Fig. 10: Using downhole RPM sensors, calculated RPM factors are constantly decreasing throughout the well indicating continuous motor damage. The most significant decrease in motor damage occurs while rotating.

Furthermore, by the end of the run, the RPM factor had decreased to ~.2 rev/gal, half the expected RPM factor of .4 rev/gal. Assuming a standard operating string rpm of 90 rpm and a standard flow rate of 750 gpm, reducing the RPM factor by 50% would reduce the overall bit speed by 38%. Not only will this reduce the theoretical ROP by 38%, it will also increase the chances of experiencing damaging stickslip and motor stalls (Ertas et al. 2013). Therefore, a deteriorating motor not only reduces performance, but may accelerate bit and motor damage by becoming more susceptible to those dysfunctions.

4. DIFFERENTIAL PRESSURE DYNAMICS

To monitor downhole dynamics, a suite of high frequency downhole sensors was run both above and below the motor to monitor.

Magnitude Response

There is a significant discrepancy in surface differential pressure when compared to downhole differential pressure. As shown in **Fig. 11** differential pressure ranges over 500 psi over fractions of a second. While this is an extreme example, it is surprisingly not uncommon. Even the most quiet high frequency responses showed that differential pressure will oscillate between 150 to 200 psi several times per second. However, while it is difficult to ascertain, these regular oscillations are probably not damaging. In fact, they likely indicate that the motor is operating efficiently. As a cavity between the rotor and the stator fills up, the pressure spikes until a new cavity becomes open. The pressure drops as the mud rushes to fill the cavity. Once full, the pressure spikes again until the next cavity is open. The lack of a regular oscillation indicates the seal between the rotor and stator has become less effective and fluid can bypass the discrete cavities, preventing regular pressure build up cycles. The more alarming observation occurs between 20 and 20.4 seconds when the average downhole differential pressure drops by ~350 psi. The surface differential pressure remains constant and shows no change.

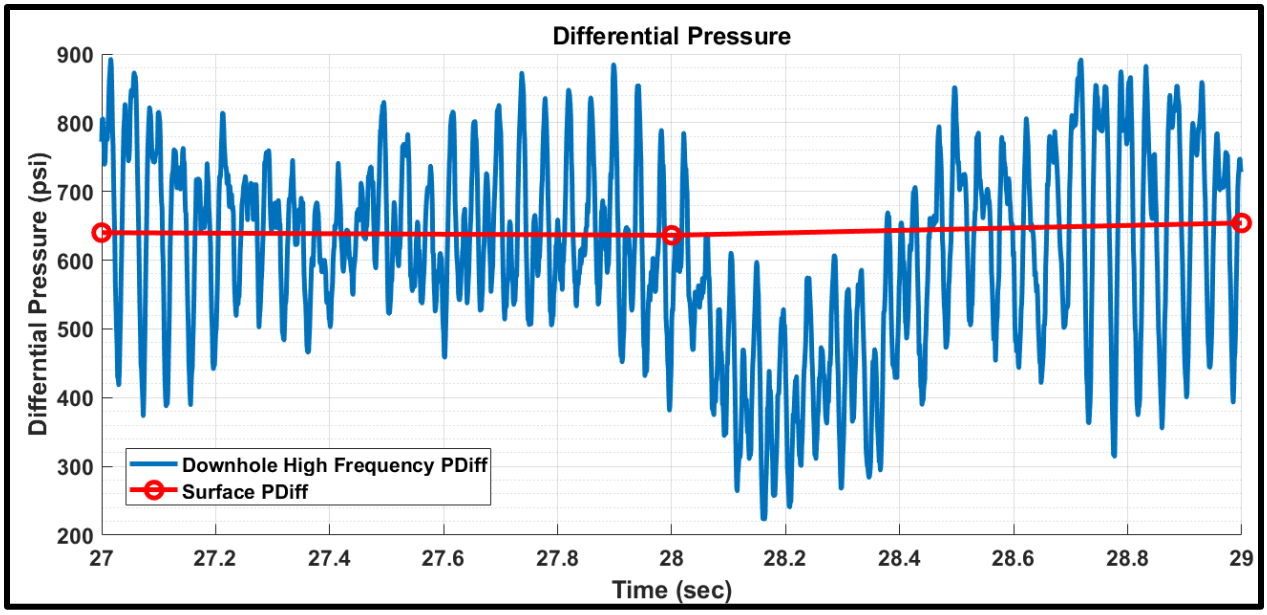

Fig. 11: Surface differential pressure is a poor indicator of actual downhole pressure.

In the case of a stall, shown in **Fig. 12,** the change in differential pressure can be even more dramatic, reaching 800 psi over 0.5 seconds. Yet, the surface data only increase by 70 psi, less than 10% of the actual increase. On a real time surface EDR, this change would be difficult to notice. When the stall is broken, this built up energy becomes violently dissipated. In all examples found in this stud, while the surface data mimics the trends, it by no means demonstrates the full severity of the extremes in differential pressure. As such, it is important for drillers to understand that any or spikes in differential pressure observed on the surface, are likely to be magnified multiple times downhole. This shows that it is possible to stall a motor even if the surface data reports a differential pressure that is still a few hundred psi below the reported stall pressure.

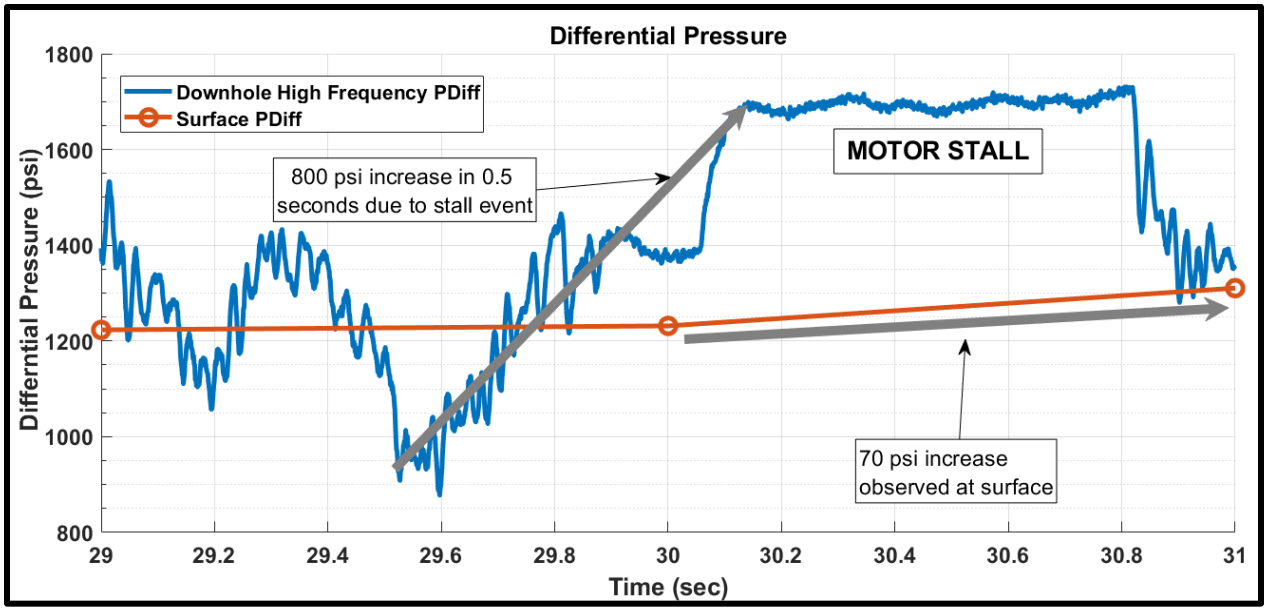

Fig. 12: During a motor stall, surface differential pressure only increases by 70 psi while downhole pressure increases by 800 psi.

Frequency Response

The oscillatory differential pressure signature was analyzed using a fast Fourier transform (FFT) to identify dominant frequency responses. As shown in **Fig. 13,** at the beginning of the run, the differential pressure FFT provided a very clear spike showing a fundamental frequency at around 25Hz. The frequency response was nearly identical for both rotating and sliding operation and clear harmonic responses can be seen at multiples of the fundamental frequency. Two key differences can be observed. First, more harmonic responses can be observed while sliding. Second, drilling while rotating increases the amplitude of the differential pressure oscillations. These can be explained by the presence of increased BHA whirl which and introduces more noise while rotating.

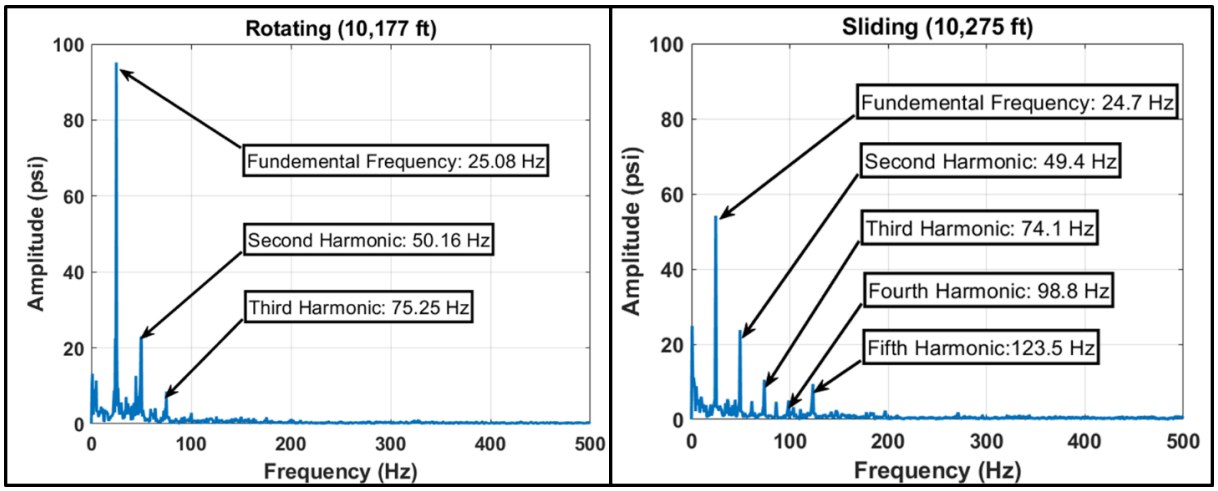

Fig. 13: FFT analysis of differential pressure at the start of the run while sliding (right) and rotating (left). Rudced noise due to reduced whirl allows for greater harmonic frequencies to be observed while sliding

This dominant frequency response can be explained by using the proposed equation shown in Eqn. 6 where 60 is a conversion factor from rpm to frequency. As the rubber becomes more damaged the output rpm will decrease and there should be an observed decrease in the fundamental frequency.

$$Fundemental\ Frequency\ = \frac{Number\ of\ Lobes\ on\ Rotor * Rotor\ RPM}{60} \quad \text{.....(6)}$$

As drilling continues the FFT signature changes in two ways. First, the frequency response becomes less clear. The first harmonic decreases in magnitude and more noise is present as represented by more minor spikes at various frequencies. **Fig. 14** shows the FFT response at the end of the curve and **Fig. 15** shows the FFT response near the end of drilling the lateral. Post-run analyses have shown that rubber chunking occurs at the bottom of the power section and works its way upward. Therefore, the lower cavities are becoming bigger as the rubber becomes chunked. The upper cavities are sending smaller fluid packets as compared to the lower cavities. These fluid packets hit the newly enlarged cavities requiring additional fluid to fill. This causes

less fluid out of the end of the motor and likely causes a miniature fluid pound effect to occur in the motor. The fluid pound in turn exacerbates wear and shows up as erratic pressure pulses.

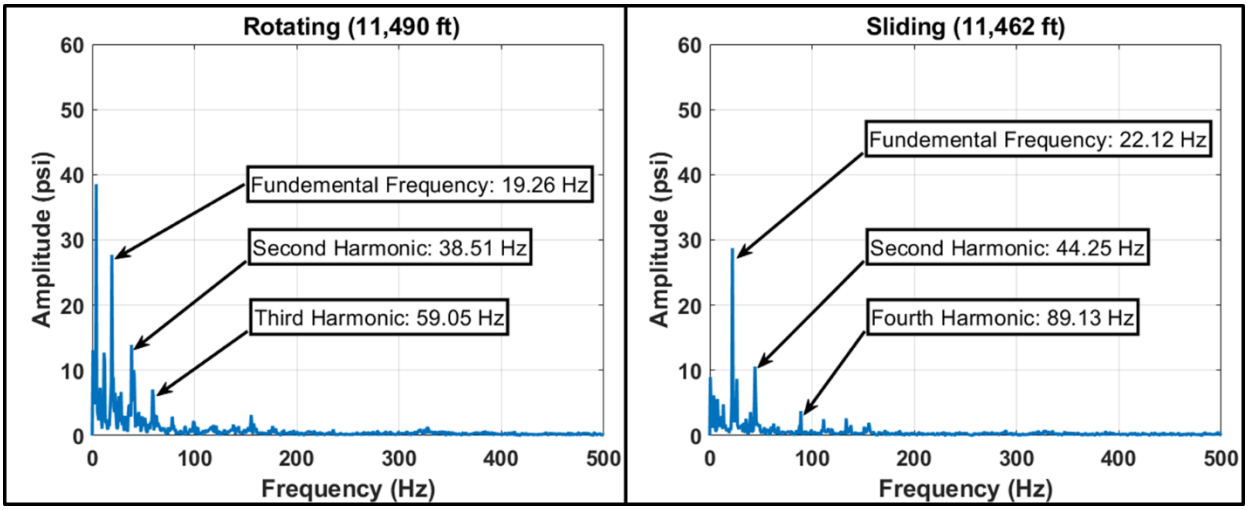

Fig. 14: FFT analysis of differential pressure in the middle of the run while sliding (right) and rotating (left). Even just 1,000' into drilling, signs of damage have become clearer as the dominant frequency magnitude has gone down significantly. Note the change in scale from Fig. 13.

The second observation is that the frequency responses between rotating and sliding no longer mimic each other once the rubber has experienced enough degree of wear, as shown in Fig 15. As the rubber chunks, the rotor is allowed more space to oscillate within the rotor. While sliding, these rotor oscillations are minimized due to reduced overall BHA whirl. However, while rotating, the mass imbalance induced whirl magnifies the rotor oscillations. These oscillations result in a noisier differential pressure FFT response and accelerate rubber damage. As more time is spent rotating rather than sliding, enacting appropriate techniques to decrease whirl can provide a more stable motor pressure response by reducing the degree of motor damage.

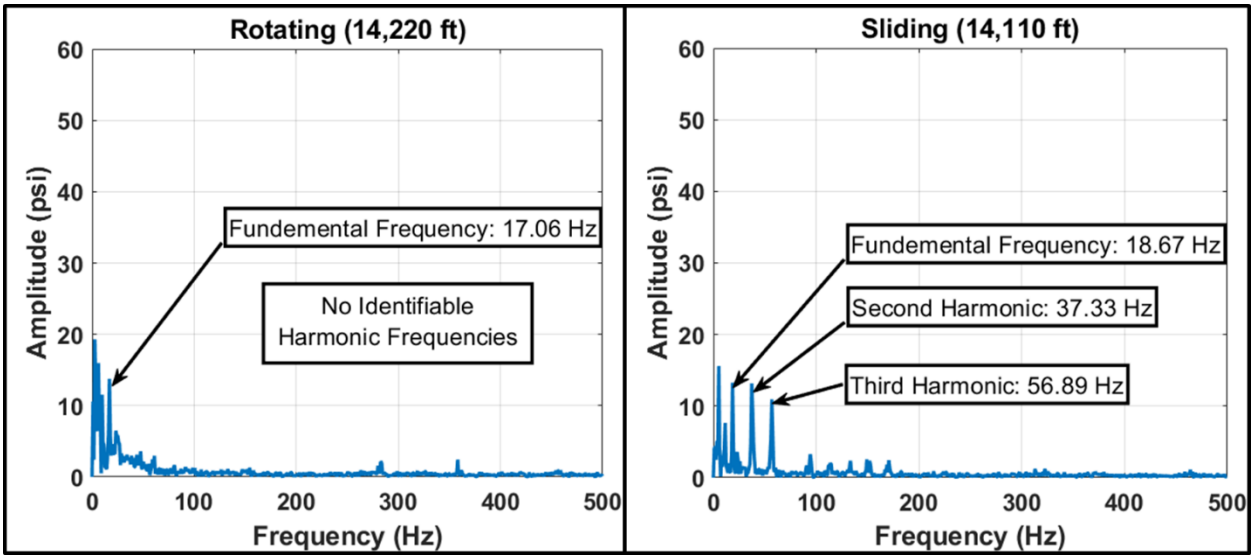

Fig. 15: FFT analysis of differential pressure at the end of the run while sliding (right) and rotating (left). Significant noise is induced into both signals. Harmonics cannot be seen in the rotating FFT. Note the change in scale from Fig. 13.

MSE Based Optimization

MSE monitoring is widely used as a technique to identify the most efficient drilling parameters with the least vibration. While proper MSE monitoring can help select the best conditions for drilling at the bit, it does not provide indication of the ideal parameters to extend motor life. **Fig 16** shows the MSE_{Bit} during a WOB step test. Based on the premise of minimizing MSE_{Bit}, the best operating condition would be at the second to last step—63 klbs—because it is the greatest WOB before MSE_{Bit} increases. In contrast **Fig. 17** shows the differential pressure FFT responses at each step test. Based on these figures, the step test that yielded the largest amplitude fundamental frequency was the first step at 43 klbs; however, there is not a significant difference between steps one through five.

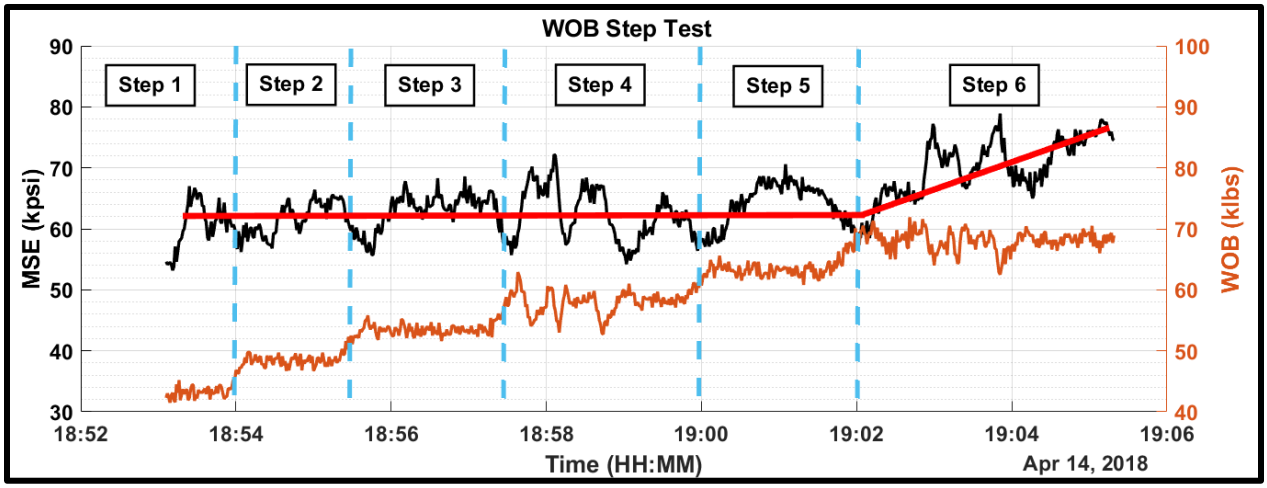

Fig. 16. WOB step test conducted suggesting a best operating condition at 63 klbs.

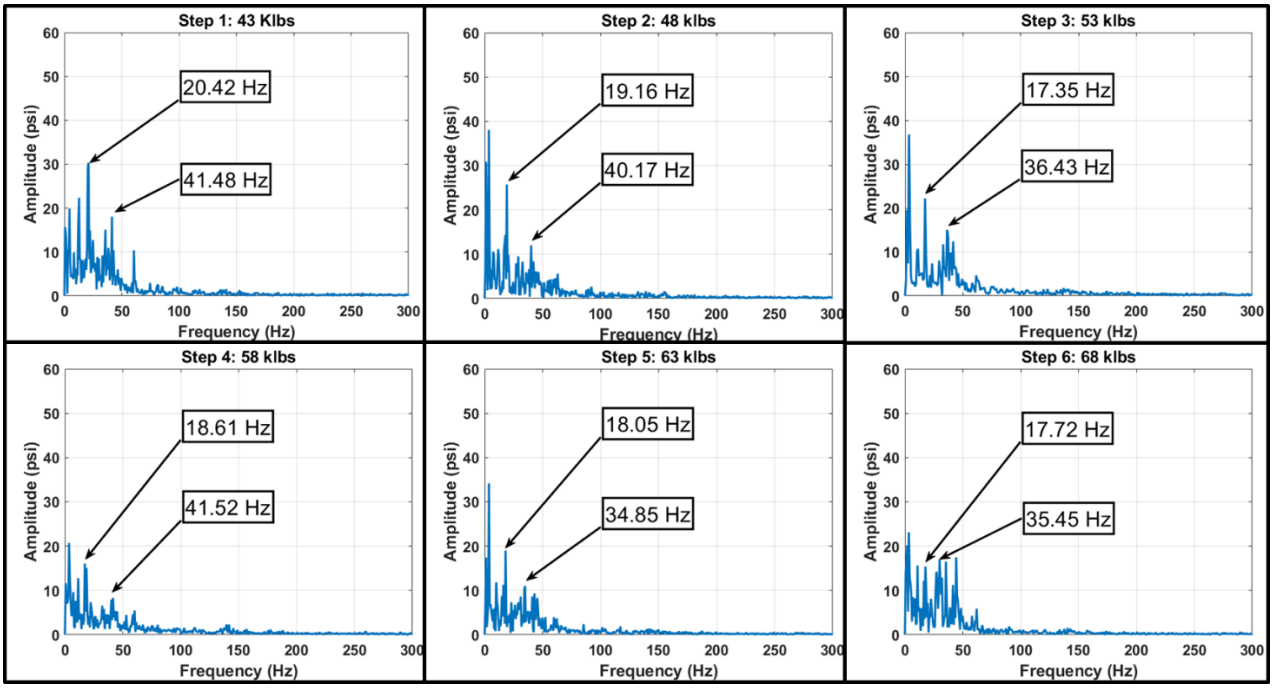

Fig. 17: FFT comparisons from the WOB step test are not definitive for steps 1-5

This position is further supported by comparing shock data measured above and below the motor with MSE_{Bit} calculated using surface data. **Fig 18a** shows that below 65 kpsi, there were no significant changes in shocks at the bit. Once MSE_{Bit} is increased past 65 kpsi, the shocks

increase as the bit reaches the founder point. In contrast, **Fig. 18b** shows that there is no clear correlation between MSE_{Bit} and the above motor shocks. Hence, while MSE_{Bit} monitoring can be used to drill faster with less dysfunction, it does not simultaneously serve as a direct indicator of the best parameters for improved motor life.

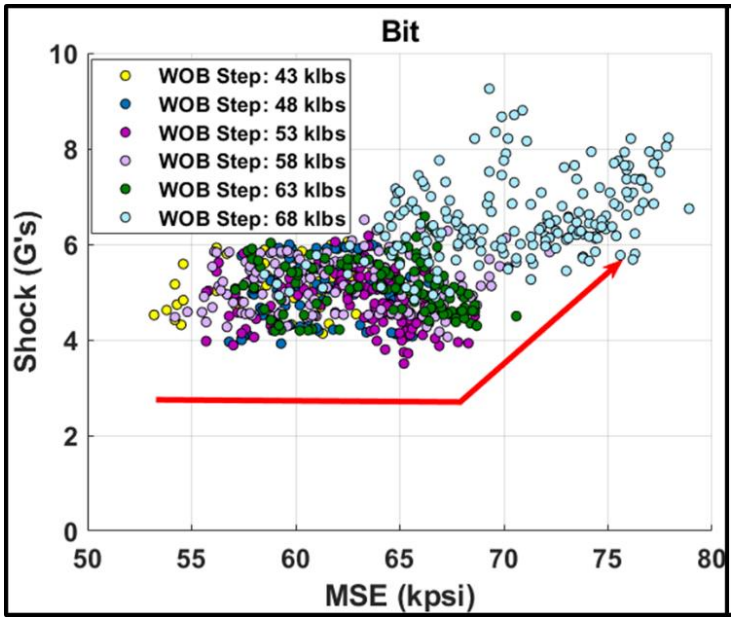

Fig. 18: Shock data at the bit shows a strong correlation with MSE_{Bit}.

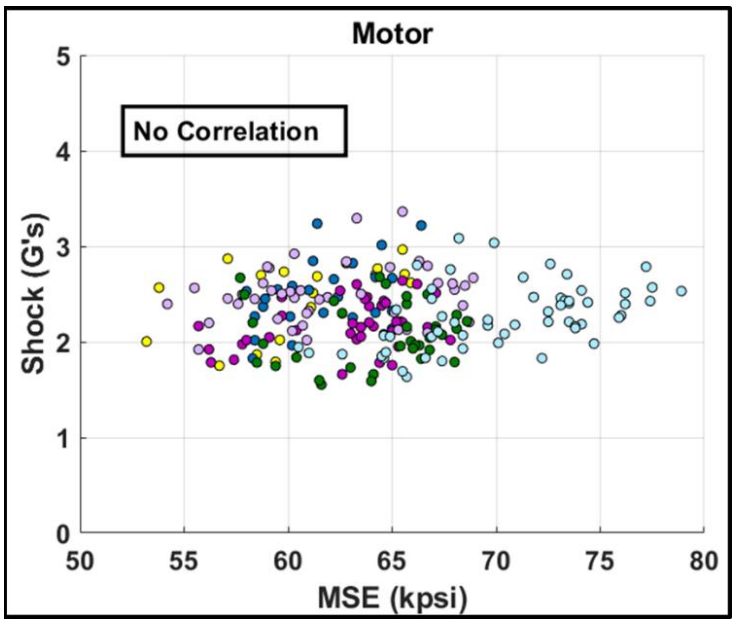

Fig. 19: Shock data at the motor shows no correlation with MSE_{Bit}.

This can be explained by the fact that fundamentally, MSE_{Bit} monitors efficiency at the bit. By increasing WOB, the bit's cutters engage the formation and whirl is suppressed. However, this does not affect the degree of whirl in the BHA or at the motor and can even make the whirling motion of the BHA itself worse (Bailey et al. 2008). Instead, different techniques must be implemented to design a BHA with reduced whirl such as proper stabilization design or a reduced bend angle motor (Hohl et al, 2017).

5. DEPTH OF CUT CONTROL

Depth of cut control (DOCC) utilizes raised features on the bit's matrix that engage with the rock formation after a certain depth of cut (DOC). Once the depth of cut is reached where the DOCC features engage, the total bit contact area with the formation increases; however, only the cutters contribute to the drilling process. The increased friction caused by the DOCC inserts results in decreased bit aggressiveness once the buttons have engaged (Detournay and Defourny 1992). The decreased aggressiveness, shown in **Fig. 20**, results in reduced torque oscillations (Ertas et al. 2013)).

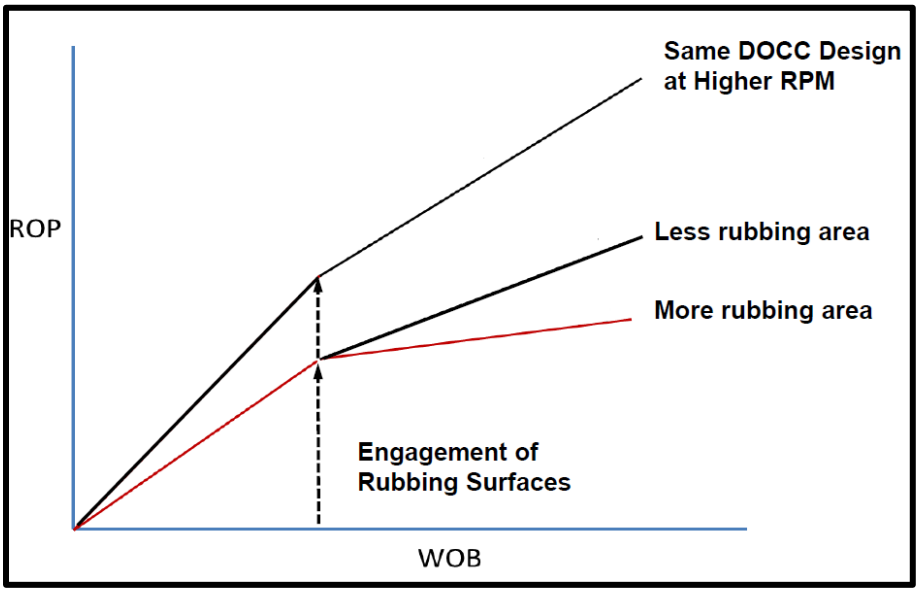

Fig. 20: After the DOCC engages, ROP will increase at a slower rate due to the decreased bit aggressiveness.

DOCC features have often been used to improve directional control and mitigate stickslip due to the reduction in torque oscillations (Ertas et al. 2013; Denney 2011; Davis et al. 2012; Barton et al. 2007). However, the proper design of a DOCC system has the potential to improve motor life due to the reduction in overall vibrations at the bit. A portion of this study included field trials to

investigate the effect of DOCC on motor life and downhole vibration mitigation. The DOCC was designed to engage at the upper limit of the operating ROP at the typical total bit speed for the interval in question. This way the bit would maintain its high aggressiveness under normal operating conditions but will engage whenever excessive overbites of the cutting structure would have occurred on previous, non-DOCC designs. The expectation was a reduction in the fluctuations in motor torque. For this application DOCC was designed to engage at 0.25 in/rev. using diamond buttons. The use of diamond over carbide is important as carbide-only DOCC will continually wear away and will not provide a consistent engagement DOC. The result of the trial was compared to a nearby well drilled on the same pad using an identical BHA and operating parameters.

Calculating the DOC of an individual cutter on a bit is a complicated task that depends on the cutter density, blade shape, and overall bit geometry. Instead it is helpful to generalize and examine the total DOC per revolution of the bit. This takes into account the effects of all cutting elements and allows for a value that can be compared across different bit types. It can be imagined as the total ROP per single revolution of the bit. Therefore, DOC per revolution for this work can be calculated using Eqn. 7 where 0.2 is a unit conversion factor.

$$DOC\ per\ revolution = 0.2 * \frac{ROP}{Bit\ RPM} \quad \text{.....(7)}$$

Fig. 21 shows calculated DOC as function of operating WOB. This plot is used to verify that the DOCC features engaged at their designed DOC. The plot was generated using data from a step test that began at 55 klbs and went up to 75 klbs. Lower value WOB data points found by analyzing the data at the start of drilling a new connection as WOB was being applied. A clear change in slope in the red line indicates that the DOCC buttons engaged at the designed DOC of ~ 0.25in/rev. This result was generated using a motor RPM factor of .28 as based on the

downhole sensor data from the prior well (Fig. 9). The same analysis performed using the reported value of 0.4 would yield a misleading DOC engagement at 0.2 in/rev as seen by the yellow line. This would lead to the incorrect conclusion that the DOCC did not perform as designed.

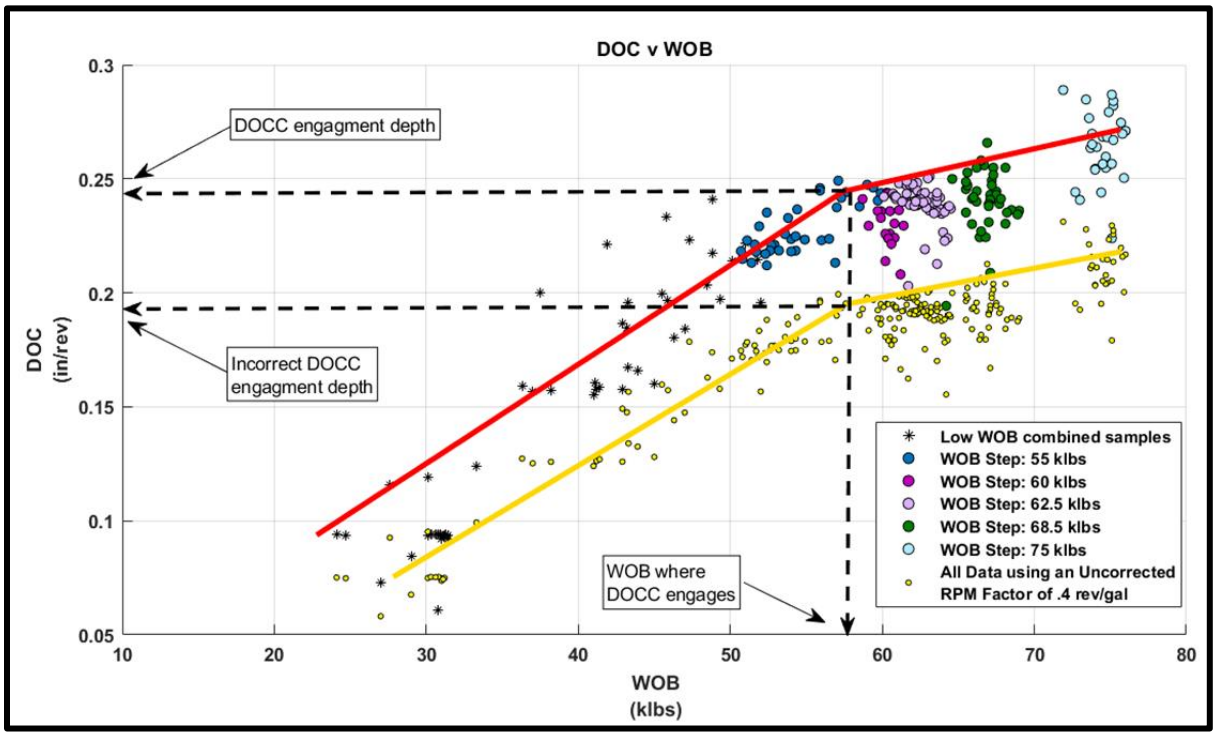

Fig. 21: DOCC engages at the designed DOC of .25 in/rev. Using the reported RPM factor results in an incorrect identification of the engagement depth.

To analyze the effectiveness of the DOCC in mitigating differential pressure spikes, a ~2,000 ft. section of the lateral was selected to be compared to a prior well that was drilled under near identical conditions (**Fig. 22**). The section began after landing the curve and ended before a downhole whirl event lead to bit damage. **Fig. 23** shows the rate of change of surface differential pressure for the wells with and without DOCC. Initially, both wells experienced similar degrees in fluctuation in differential pressure. However, halfway through the interval in question, the

fluctuations in the well without DOCC increased whereas the well with DOCC remained relatively constant. A statistical approach verifies these observations. **Fig. 24** shows that the standard deviation for the well drilled without DOCC increased with time and was noticeably greater than the standard deviation for the well drilled with DOCC. Even though the changes in differential pressure seem minimal in Figs. 21 and 22, small oscillations in surface measurements correspond to high frequency swings in the hundreds of psi. Even small changes on a linear scale are significant. Thus, the increased deviation in differential pressure can be explained by rubber fatigue and potential damage onset. A standard EDR display will only show the differential pressure as showing in Fig. 21. By simply looking at that plot, it is not clear to a driller that there is a significant decrease in the rate of change of differential pressure oscillations.

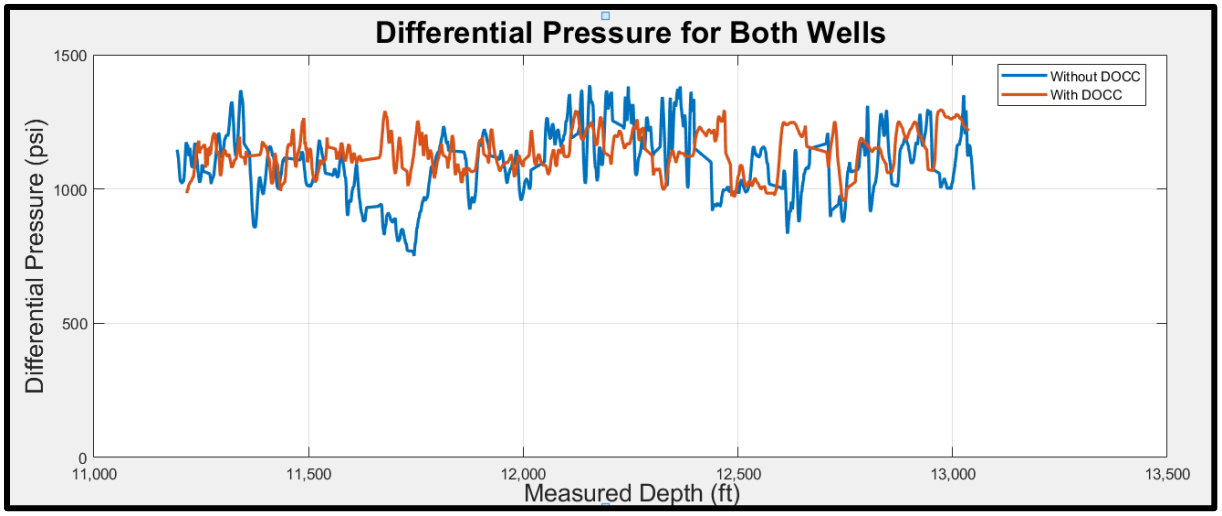

Fig. 22: Surface differential pressure data for both wells. Both wells were operating under similar conditions. However, surface data lone does not demonstrate a clear difference in motor performance.

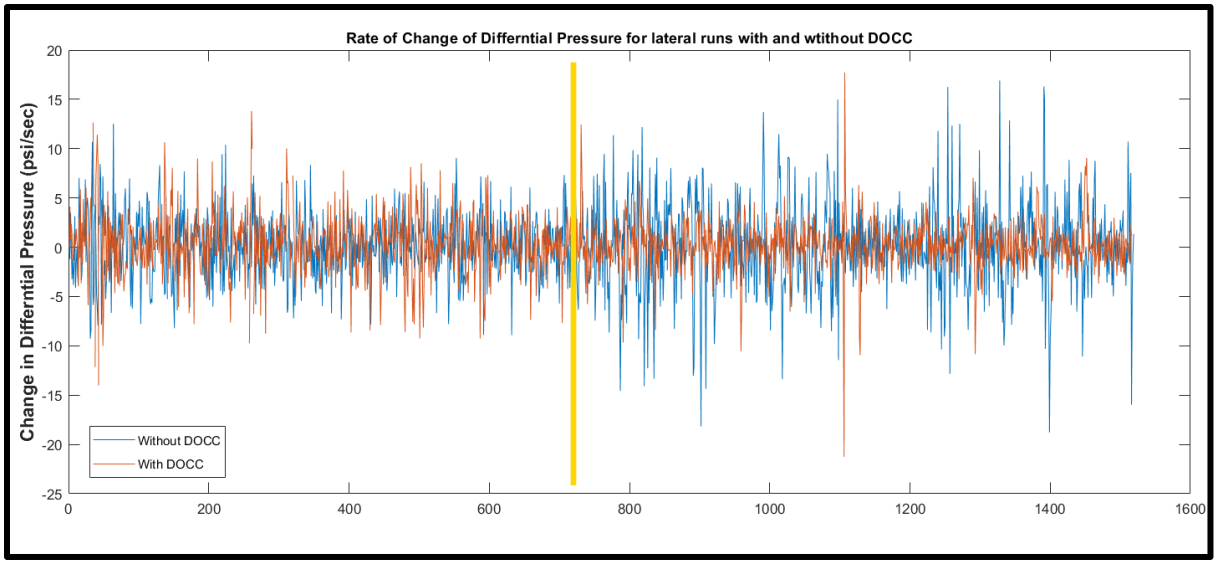

Fig. 23:The change in differential pressure appears identical in the first half (left of the line) but then changes differences are more pronounced the second half (right of the line) of the lateral.

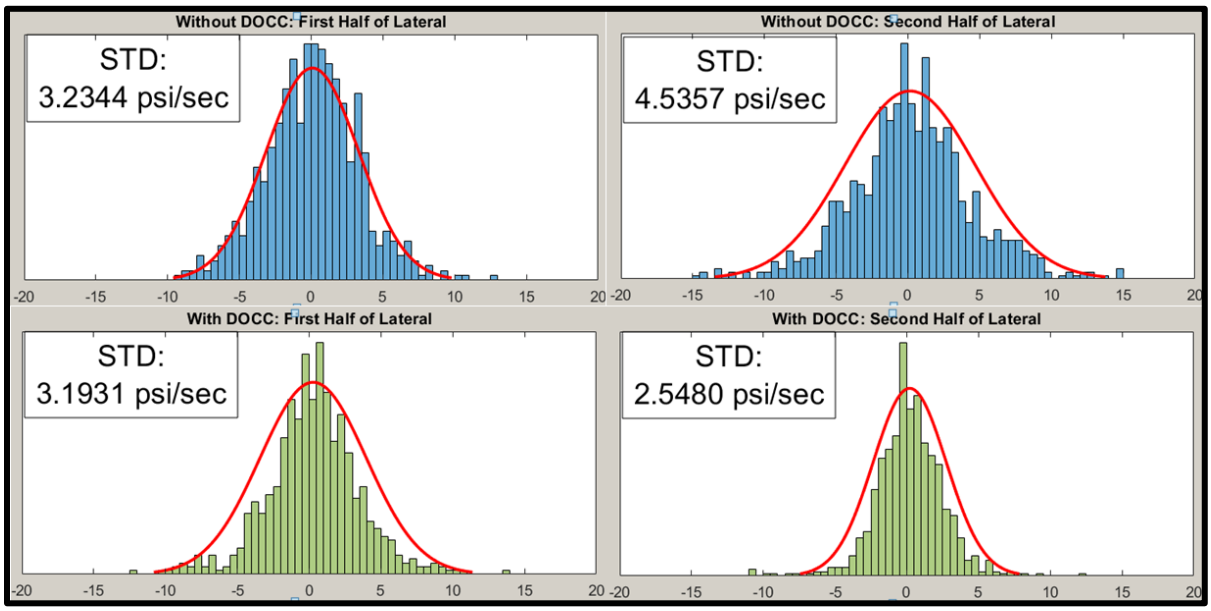

Fig. 24: The standard deviation of the derivative of differential pressure are a better indication effectiveness of DOCC in reducing differential pressure oscillations.

6. CONCLUSION

Downhole sensors were run to analyze the performance of mud motor power sections and the reliability of using MSE_{Bit}. If the reported rpm and torque factors are accurate, they can be used to calculate MSE with minimal error. Service providers can reduce this degree of error by reporting RPM factors at realistic loads rather than no load factors. However, power section degradation due to operation can yield significant decreases in RPM factors and consequently bit rpm. This not only reduces ROP but makes the BHA more susceptible to stalls and stickslip. Moreover, an analysis of high frequency downhole differential pressure shows that surface data is a poor indicator of the real swings in differential pressure downhole, which can reach 500 psi over a fraction of a second. In addition, the frequency response of differential pressure can provide an indication of the integrity of the rubber. An equation was suggested that predicts the dominant differential pressure frequency given the stator rpm and number of lobes. Despite this, MSE_{Bit} is not a good indicator of the best operating differential pressure to preserve motor life. Rather specific changes must be enacted to reduce overall motor vibrations.

Calculating the rpm factors on the operator's wells using actual motor speeds show that motor degradation is a significant problem, resulting in a reduction of up to 40% in bit RPM. The greatest drop in the rpm factors occurs in the lateral section of the well rather than the curve. This is attributed to the increase of rotating as compared to sliding. While rotating, the motor experiences significantly more whirl due to the bend angle. While it is not possible to eliminate rotating from the lateral, it is possible to redesign the BHA to reduce the overall whirl improve motor performance. Proper stabilization and the use of a lower bend angle are the two discussed approaches. Reducing the bend angle below the already high 2.12° has the added advantage of

allowing a greater string rpm, which would offset the reduction in rotor rpm due to rubber degradation.

The reduction in the actual rpm factor from the expected rpm factor during the lateral can also be used to correlate the degree of motor damage in realtime if motor speed can be measured in realtime. Monitoring motor damage realtime would be a strong addition to a driller's toolbox, providing them with information to improve performance. Real time motor rpm can be measured by a downhole sensor and sent to the surface at a low frequency via mud pulse telemetry. Alternatively, the differential pressure can be measured at a high frequency at the standpipe to identify the fundamental frequency response. This in turn provides an accurate representation of the motor speed.

Lastly, the use of properly designed DOCC was suggested as a means to decrease the differential pressure fluctuations on the power section and increase motor longevity. The use of the wrong rpm factor, and therefore the wrong bit speed, may mislead conclusions regarding whether the design behaved correctly. Comparing two wells, the well that featured DOCC outperformed the control well in regards differential pressure oscillation. Furthermore, analyzing the standard deviation of the first derivative of differential pressure, is used as an improved way to quantify and visualize the effect of DOCC beyond what can be seen in EDR displays.

Taking the necessary steps to improve motor integrity can extend the life of a motor and postpone failure. Perhaps more importantly however, is that by reducing the degree of damage in the motor, operators will be able to drill faster due to the preservation of rpm. Much of this study focused on a few key wells to derive understanding of mud motor operations. While key insights are explored, the work would benefit from additional application across multiply wells to solidify the findings.

REFERENCES

Ba, S.A., Pushkarev, M., Kolyshkin, A. et al. 2016. Positive Displacement Motor Modeling: Skyrocketing the Way We Design, Select, and Operate Mud Motors. Presented at the Abu Dhabi International Petroleum Exhibition and Conference, Abu Dhabi, United Arab Emirates, 7—10 December. SPE-183298. http://dx.doi.org/10.2118/183298.

Bailey, J., Biediger, E., Sundararaman, S. et al. 2008. Development and Application of a BHA Vibrations Model . Presented at the International Petroleum Technology Conference, Kuala Lumpur, Malaysia, 3—5 December. IPTC-12737. http://dx.doi.org/doi:10.2523/IPTC-12737-MS.

Barton, S.P., May, H.S., and Johnson, S. 2007. Gauge, Cutting structure, Torque Control Components - What really Counts for Optimal Tool Face Control with FC drill bits?. Presented at the Rocky Mountain Oil&Gas Technology Symposium, Denver, Colorado, 16—18 April. SPE-107289. http://dx.doi.org/10.2118/107289.

Beeh, H.A., Nobre, D., Ba, S. et al. 2018. Drilling a Challenging Kvitebjørn Field 5¾-in. Section in a Single Run Using a New Mud Motor Modeling Engineering Workflow and New Long-Life Elastomer. Presented at the SPE Norway One Day Seminar, Bergen, Norway, 18—18 April. SPE-191331. http://dx.doi.org/10.2118/191331.

Bybee, K. 2010. The Performance of Mud Motors With Two Different Bent Housings. Journal of Petroleum Technology 62 (12): 84—86. SPE-1210-0084. http://dx.doi.org/10.2118/1210-0084.

Davis, J., Smyth, G.F., Bolivar, N. et al. 2012. Eliminating Stick-Slip by Managing Bit Depth of Cut and Minimizing Variable Torque in the Drillstring. Presented at the IADC/SPE Drilling Conference and Exhibition, San Diego, California, 6—8 March. SPE-151133. http://dx.doi.org/10.2118/151133.

Detournay, E. and Defourny, P. 1992. A Phenomenological Model for The Drilling Action of Drag Bits. Oil & Gas Facilities 29 (1): 13—23.

Delpassand, M.S. 1999. "Stator Life of a Positive Displacement Downhole Drilling Motor." J. Ener Res Technol 121 (2): 110-116.

Denney, D. 2011. Mitigating Torsional Stick/Slip Vibrations in Oilwell Drilling Through PDC-Bit Design: Putting Theories to the Test. Journal of Petroleum Technology 63 (12): 79—80. SPE-1211-0079. http://dx.doi.org/10.2118/1211-0079.

Dupriest, F. and Koederitz, W. 2002. Maximizing Drill Rates with Real-Time Surveillance of Mechanical Specific Energy. Presented at the SPE/IADC Drilling Conference, Amsterdam, Netherlands, 23—25 February. SPE-92194. http://dx.doi.org/10.2118/92194.

Dyck, T. 2011. Motor Handbook, seventh edition. Houston, Texas: National Oilwell Varco.

Ertas, D., Bailey, J., Lei, W. et al. 2013. Drillstring Mechanics Model for Surveillance, Root Cause Analysis, and Mitigation of Torsional and Axial Vibration. Presented at the SPE/IADC Drilling Conference, Amsterdam, Netherlands, 5—7 March. SPE-163420. http://dx.doi.org/10.2118/163420.

Fei, Z., Haige, W., Meng, C. et al. 2017. Monitoring and Mitigating Downhole Vibration With MSE in XinJiang Oil Filed of China. Presented at the 51st U.S. Rock Mechanics/Geomechanics Symposium, San Francisco, California, 25—28 June. ARMA-2017-0694. http://dx.doi.org/10.2118/ARMA-2017-0694.

Gamboa, J., Olivet, A., Iglesias, J. et al. 2003. "Understanding the Performance of a Progressive Cavity Pump with a Metallic Stator." Proceedings of the Twentieth International Pump Users Symposium. 19-31.

Guidroz, B., Barton, S., and Hussain, M. 2011. SPE Annual Technical Conference and Exhibition. Presented at the SPE Annual Technical Conference and Exhibition, Denver, Colorado, 30 October—2 November. SPE-146575. http://dx.doi.org/10.2118/146575.

Hendrik, J. 1997. Elastomers in Mud Motors For Oil Field Applications. Presented at the Corrosion97, New Orleans, Louisiana, 9—14 March. NACE-97085.

Hohl, A., Hohl, C., & Herbig, C. et al. 2015. A Combined Analytical and Numerical Approach to Analyze Mud Motor Excited Vibrations in Drilling Systems, In ASME Turbo Expo 2015: Turbine Technical Conference and Exposition, Quebec, Canada, 15—19 June. http:// doi:10.1115/GT2015-42144

Hohl, A., Hohl, C., and Herbig, C. 2017. Characterization and Mitigation of Mud Motor Vibrations. Presented at the SPE/IADC Drilling Conference and Exhibition, The Hague, Netherlands, 14—16 March. SPE-184711. http://dx.doi.org/10.2118/184711.

Jaeger, T., Herlitzius, J., 2016. Navi-Drill Motor Handbook, Vol. 13. Baker Hughes Incorporated, Celle.

Macpherson, J.D. and Jogi, P.N. 2001. Measurement of Mud Motor Rotation Rates using Drilling Dynamics. Presented at the SPE/IADC Drilling Conference, Amsterdam, Netherlands, 27 February—1 March. SPE-183298. http://dx.doi.org/10.2118/183298.

Moineau, R., 1939. "A new capsulismus". PhD thesis, University of Paris, France.

Pessier, R.C. and Fear, M.J. 1992. Quantifying Common Drilling Problems With Mechanical Specific Energy and a Bit-Specific Coefficient of Sliding Friction. Presented at the SPE

Annual Technical Conference and Exhibition, Washington D.C, District Of Columbia, 4—7 October. SPE-24584. http://dx.doi.org/10.2118/24584.

Rafatian, N., Miska, S.Z., Ledgerwood, L.W. et al. 2009. Experimental Study of MSE of a Single PDC Cutter Under Simulated Pressurized Conditions. Presented at the SPE/IADC Drilling Conference and Exhibition, Amsterdam, Netherlands, 17—19 March. SPE-119302. http://dx.doi.org/10.2118/119302.

Remmert, S.M., Witt, J.W., and Dupriest, F.E. 2007. Implementation of ROP Management Process in Qatar North Field . Presented at the SPE/IADC Drilling Conference, Amsterdam, Netherlands, 20—22 February. SPE-105521. http://dx.doi.org/10.2118/105521.

Samuel, G.R. and Miska, S. 1997. Analytical Study of the Performance of Positive Displacement Motor (PDM): Modeling for Incompressible Fluid. Presented at the 5th Latin American Caribbean Petroleum Conference&Exhibition, Rio de janeiro, Brazil, 30 August—3 September. SPE-39026. http://dx.doi.org/10.2118/39026.

Teale, R. 1965. The Concept of Specific Energy in Rock Drilling. Intl. J. Rock Mech. Mining Sci. 2. 57-73.